Construction and Building Materials 409 (2023) 133879

Contents lists available at ScienceDirect

Construction and Building Materials

journal homepage: www.elsevier.com/locate/conbuildmat

Cleaner, sustainable, and safer: Green potential of alkali-activated materials in current building industry, radiological good practice, and a few tips

Laura Tositti [a,*], Giulia Masi [b], Pietro Morozzi [a], Alessandro Zappi [a], Maria Chiara Bignozzi [b,*]

[a] Department of Chemistry "G. Ciamician", University of Bologna, Via Selmi 2, 40126 Bologna, Italy
[b] Department of Civil, Chemical, Environmental and Materials Engineering (DICAM), University of Bologna, Via Terracini 28, 40131 Bologna, Italy

ARTICLE INFO

Keywords:
Geopolymer
Alkali activated material
Natural radionuclides
NORM
Dosimetric index
High-resolution gamma-ray spectrometry

ABSTRACT

Alkali-activated materials were prepared from four typical precursors (coal fly ash, granulated blast furnace slag, metakaolin, and brick waste powder) characterized for granulometry, elemental composition, and microstructure. High-resolution gamma-ray spectrometry was used to determine the activity concentration of Naturally Occurring Radioactive Materials (NORM) in all the materials to assess their radiological impact. All the investigated materials have been found to comply with the European dosimetric index (I) according to Directive 2013/59/Euratom. The results suggest the need for an accurate check of radioactivity throughout the mixing phases to prevent I exceedances. The productive chains were also evaluated by principal component analysis.

1. Introduction

The current environmental and climatic constraints are urging towards increasingly efficient and sustainable materials and production processes, leading to a reduction of exploited natural resources, processing emissions as well as wastes [1].

Within the building industry, alkali-activated materials (AAMs) and geopolymers are increasingly gaining in attractiveness for their numerous advantages [2]. In particular, the production of these materials allows for a substantial reduction in CO_2 emissions, due to the production processes not requiring calcination of the carbonate component, rarely present in the raw materials, and lower energy costs, due to the lower process temperature, thus involving even lower fossil fuel emissions [3].

Moreover, the starting materials employed are increasingly introducing industrial solid wastes deriving from mineral origin such as, for example, energy production based on coal fly ash or from metal smelting. At the end of the primary industrial cycles, a geogenic-like matrix is somehow preserved, suggesting waste recycling as an alternative route to produce building materials [4,5].

AAMs and geopolymers are defined as inorganic aluminosilicate binders [6]. Despite the first publication on this topic being dated back to 1979, the research interest is steadily increasing since 2000 [4,5,7], thanks to the outstanding performances in terms of mechanical strength, high-temperature resistance, durability, and environmental sustainability measured for optimized formulation [8]. Provis [8] defined this class of materials as sustainable binder systems with different features compared to traditional cementitious materials, but with important characteristics, such as versatility and local adaptability. To prepare AAMs and geopolymers, a wide range of recycled precursors can be used. The most used raw materials in research are sourced by industrial by-products, i.e., fly ash derived from coal combustion or slag from iron-making production [8,9]. However, since precursors for AAMs are defined as aluminosilicate materials rich in amorphous SiO_2 and Al_2O_3, a wide range of urban and industrial by-products can be promisingly applied for alkali activation, such as ash from municipal waste incineration, demolition, and ceramic waste from the building sector, sediments from water treatment plants (sewage sludge) and waste from agriculture and mineral industry [9]. One of the most interesting aspects of the precursor selection is the possibility to use locally available materials, thus allowing to minimize the transportation of raw materials and to reduce the landfilled materials [8,10]. This approach would reduce the environmental impacts of the final products because usually transport phases strongly reduce environmental sustainability [8,11]. On the other hand, the wide range of potential precursors with different mineralogical/technogenic sources, chemical composition, shape, and grain size, slow down the development of universal formulations, such as in the case of cementitious materials. For this reason, mix design

* Corresponding authors at: Via Selmi 2, 40126, Bologna, Italy (L. Tositti); Via Terracini 28, 40131 Bologna, Italy (M.C. Bignozzi).
E-mail addresses: laura.tositti@unibo.it (L. Tositti), giulia.masi5@unibo.it (G. Masi), pietro.morozzi2@unibo.it (P. Morozzi), alessandro.zappi4@unibo.it (A. Zappi), maria.bignozzi@unibo.it (M. Chiara Bignozzi).

https://doi.org/10.1016/j.conbuildmat.2023.133879
Received 20 June 2023; Received in revised form 10 October 2023; Accepted 18 October 2023
Available online 21 October 2023

optimization is a fundamental process in the development of AAMs [7,8,10]. Thus, a precise tailoring of the alkaline activators (i.e., alkali metal hydroxide and silicates), usually aqueous solutions, but also solid activators to produce the so-called "one-part geopolymers" [4] is necessary to optimize the properties of the final products. As construction materials, AAMs are usually produced as normal- or light-weight binders or mortars, and concrete by adding natural or recycled aggregates with different particle size distributions in the mixtures.

Overall, the use of AAMs highlights the achievement of at least two basic targets in terms of sustainability, i.e., a reduction in warming potential contribution as well as a reduction in solid waste management. As far as the latter factor is concerned, recent literature suggests that, besides contributing to the decrease of solid waste disposal by landfilling, AAMs from waste materials are proving chemically safe, with negligible to a null tendency to release hazardous components, as compared to parent materials, usually affected by leaching [12]. The intrinsic properties of AAMs, in this respect, are so valuable that they are being even proposed as efficient immobilizing agents for radioactive wastes [13].

Recycled waste materials, indeed, may represent a potential hazard [14] since productive processes involve the redistribution and concentration of specific trace species originally occurring in the raw material and subsequently transferred to the final product, and/or to wastes and emissions according to their physicochemical properties leading to the need for treatment, mitigation, and disposal in agreement with environmental requirements and law restrictions [14].

The raw material of mineral/lithogenic origin always includes naturally occurring radionuclides mainly associated with the three radioactive families of ^{238,235}U and ^{232}Th, beside a few primordial radionuclides, the most important of which is ^{40}K constituting a constant though small radioisotopic component of natural potassium [15,16]. Owing to their ubiquity in terrestrial rocks and soils, all these materials are defined as Naturally Occurring Radioactive Materials (from now on NORM) at highly variable concentration levels in the lithosphere and pedosphere.

It is well recognized, indeed, that rocks and minerals present variable NORM ranges as a function of the type of rock, formation process, and crystalline properties, representing overall what can be referred to as "geodiversity" [17]. Details about these aspects are extensively reported, for example, in Schön, 2015 [16]. As a result, radiation doses from the natural environment are continuously assessed and updated, while the dosimetric role of building materials, ranging from the direct use of stones or by rock composites obtained by milling and mixing into bricks, tiles, and concrete building materials, are long being investigated and checked for their radioactivity level [2,7,12]. It is to note however, that though average NORM concentration ranges in rocks can be used for classifying rocks and their geochemistry, natural radioactivity is highly variable even among single lithogenic classes as a result of the complex biogeochemistry they undergo at the geological time scale. Radioactivity in building materials is being increasingly investigated owing to the enforcement of the Euratom Directive 2013/59 and related radioprotection constraints. Main recent sources of information and data can be found in numerous publications [18–22]. In addition to natural diversity, recent exploitation of any type of resources at the planetary surface may further contribute to alter the original composition of geogenic solids, according to the environmental physico-chemical modifications brought by extraction, mining, processing, and disposing.

Both geological materials in their wide range of activity concentration levels and the exploitation of mineral resources in industrial activities have been long recognized as potentially significant radiation sources leading to excess radiation doses with respect to average population exposure [23]. In particular, the cited document highlights how both raw materials and wastes may be enriched in NORM, leading to excess radiation doses at various stages of a given production process as in the case of phosphate fertilizers and zircon sands in the ceramic tiles industry [15,24]. Elements and radioisotopes in raw materials may also undergo fractionation and/or enrichment both in the final product and in the solid wastes, owing to the specific processing they undergo. Solid wastes produced from lithogenic materials are often remarkably more radioactive than parent materials such as the well-known coal fly ash, phosphogypsum, or red muds respectively from coal burning, phosphate fertilizer cycle from apatite, and aluminum production [23,25]. Since these wastes are associated with enhanced radioactivity due to the industrial processes, the concept of Technologically Enhanced Naturally Occurring Radioactive Materials (TENORM) was introduced, together with the need for assessing the resulting contribution to the overall radiation dose.

So far, only few studies are reported in the literature on radiological AAM characteristics. They mainly deal with very peculiar precursors such as red mud, post-production clay, olive biomass ash, and radioactive precursors [26–31].

The innovation of this work is that we investigate for the first time the behavior of NORM in AAMs and geopolymers based on the most popular industrial solid wastes precursors (metakaolin, coal fly ash, ground granulated blast furnace slag and ceramic waste powder) to assess their compliance to the radioprotection regulations recently updated within the EU, according to the Council Directive 2013/59/Euratom [25] and introduced into the Italian regulation as the D.L. 101, 31st July 2020) [32]. These regulations include among others the need to assess NORM in all the building materials owing to the role they may have on the average radiation dose of the population in terms of gamma irradiation potential as well as of radon emissivity. These aspects are especially important in indoor conditions where radiation dose depends on exposure duration to direct gamma (γ) irradiation by building materials as well as to radon progeny emanation and subsequent inhalation, in connection with indoor ventilation conditions.

This paper covers the systematic analysis of high-resolution γ-ray spectra from four series of AAMs including also all the starting materials and the alkaline sources for activation of the waste precursors. The samples were characterized for their specific NORM composition and concentration level throughout the alkali activation process, and their respective dosimetric index I as from the Euratom regulation was calculated to assess their compliance with the radioprotection safety requirements.

Multivariate analysis based on Principal Component Analysis (PCA) was applied to the collected radiometric dataset to assess their relative differences and explore the potential for systematic classification purposes in the field of building materials.

2. Materials and methods

2.1. Materials

Different precursors were selected for the preparation of alkali-activated binders and mortars based on previous studies [33–38]. Class F (according to ASTM C618 standard) fly ash (FA), kindly supplied by BauMineral (EFA-Füller®, Germany), ground granulated blast furnace slag (GGBS), kindly supplied by ECOCEM (France), and brick waste powder (BWP), kindly supplied by Wienerberger S.p.A. from the industrial plant of Villabruna di Feltre, Belluno, Italy, were chosen as waste-derived precursors, while metakaolin produced by flash calcination (MK) and kindly supplied by ARGECO Dévelopement (France) was used as reference precursor. Table 1 reports the oxide composition in wt % of the different materials measured by Inductively Coupled Plasma-Optical Emission Spectrometry (ICP-OES, PerkinElmer, AVIO 550 Max). The chemical composition of the precursors represents the starting point for the mix design optimization for alkali activation. While MK and FA are mainly aluminosilicate sources ($SiO_2 + Al_2O_3 \approx 80$ % for FA and $SiO_2 + Al_2O_3 > 90$ % for MK) with low amounts of CaO and Fe_2O_3, BWP shows almost the same concentration of SiO_2, with lower concentrations of Al_2O_3 and CaO but close between them. GGBS resulted very rich in CaO, representing more than 50 % of the composition.

Table 1
Chemical composition (wt%) of the different precursors measured by ICP-OES (LOI = loss of ignition).

Precursor	SiO_2	Al_2O_3	CaO	Na_2O	MgO	TiO_2	Fe_2O_3	K_2O	SO_3	LOI
FA	56.0	22.8	5.8	0.9	1.7	0.9	6.1	1.1	0.9	2.7
GGBS	37.5	3.3	54.0	<0.01	1.0	0.7	0.4	0.4	1.9	0.4
BWP	57.7	12.5	13.3	0.2	2.9	0.5	3.2	2.4	2.5	4.3
MK	72.0	22.1	0.4	<0.1	<0.1	0.9	1.6	0.3	<0.01	2.4

Besides the chemical composition, the four precursors differ also in terms of particle size distribution and particle shapes, as reported in Fig. 1 and Table 2. In particular, Table 2 reports the main parameters related to particle size distribution in terms of the median value (d(50)) and the values of particle size for which 10 % or 90 % of the sample is smaller, namely d(10) and d(90). These data were collected using a laser scattering grain sizer (Mastersizer 2000, Malvern). GGBS exhibits the smallest particle size among the selected precursors and FA shows a comparable median value of about 15 μm but broader particle size distribution compared to GGBS. On the other hand, BWP and MK have comparable particle size distributions with a median particle size of 41 μm (Fig. 1a).

Fig. 1b reports the microstructure of the four precursors acquired by scanning electron microscopy using a field emission gun instrument (FEG-SEM, Tescan Mira3). Morphological observation highlights the typical features in terms of shape and size of the particles. While FA exhibits mostly spherical morphology (as detected elsewhere [39]), GGBS and BWP show irregular shapes, characterized by sharp edges. Finally, MK exhibits flake-like morphology, as also reported in a previous study [35].

AAMs were prepared by addition of activators and silicate components. To activate the selected precursors, different alkaline solutions were used. Sodium hydroxide (NaOH) was used in pellets (supplied by Sigma Aldrich, ACS reagent, assay ≥ 98 %) to be dissolved in sodium silicate solution or to prepare an 8 M−solution (320 g of NaOH was dissolved in 1L deionized water). The sodium silicate solution (Na_2SiO_3 supplied by Ingessil s.r.L., Italy) used for the activation shows a composition of 29.9 % SiO_2, 14.4 % Na_2O, and 55.7 % H_2O. Lastly, among the activators used for BWP, anhydrous sodium aluminate ($NaAlO_2$ supplied by Sigma Aldrich, technical grade) was used to adjust the Al_2O_3 content of the alkali-activated mixes. When mortars were prepared, standard siliceous sand (SiO_2 > 96 wt%) with a fixed grain size distribution (d_{max} = 2 mm) according to EN 196–1:2016 [40] was added as fine aggregate.

2.2. Sample preparation

The preparation of AAMs follows the scheme reported in Fig. 2.
In this work, four types of AAMs were prepared using three different precursors: two industrial wastes and metakaolin, which is the most typically used material for alkali activation technology [7]. Alkali-activated binders and mortars were prepared considering optimized mix designs from previous studies [33,34,36,37]. Mass compositions of the different components used to prepare paste and mortar samples are reported in Table 3. Samples were named using a P or M that stands for alkali-activated "paste" or "mortars", respectively, followed by the acronym used for identified the used precursor for the alkali activation (i.e., FA = fly ash, GGBS = ground granulated blast furnace slag, BWP = brick waste powder, MK = metakaolin). All samples were cured at room temperature in sealed conditions by closing the samples in plastic bags for all the curing periods.

Table 2
Main parameters of the particle size distribution of the different precursors.

Precursor	d(10) [μm]	d(50) [μm]	d(90) [μm]
FA	1.8	15.7	83.9
GGBS	3.1	13.6	33.1
BWP	5.9	41.1	139.9
MK	6.4	41.9	121.1

2.3. Characterization

2.3.1. High-resolution gamma-ray spectrometry

All the determinations were carried out after 28 days of curing in sealed conditions. Activity concentration levels of NORM in raw material and finite products were determined by high-resolution gamma-ray spectrometry. Samples were analyzed with a p-type HPGe coaxial detector (PROFILE, Ortec-Ametek Inc.) with an extended energy range (20–2000 keV). The detector has a relative efficiency of 38 %, and resolution (FWHM) at 1332.5 keV of 1.8 keV. The system was calibrated for energy and efficiency using a liquid standard source (Eckert & Ziegler Multinuclide standard solution 7501) in a jar geometry (diameter = 56 mm; thickness = 10 mm) for quali-quantitative analysis. Spectra were acquired for 1 day to optimize peak analysis. Spectra were subsequently processed and analyzed with the Gamma Vision-32 software package (version 6.08, Ortec-Ametek Inc.). ^{226}Ra was determined at 186 KeV correcting the peak area by the ^{235}U interference according to the

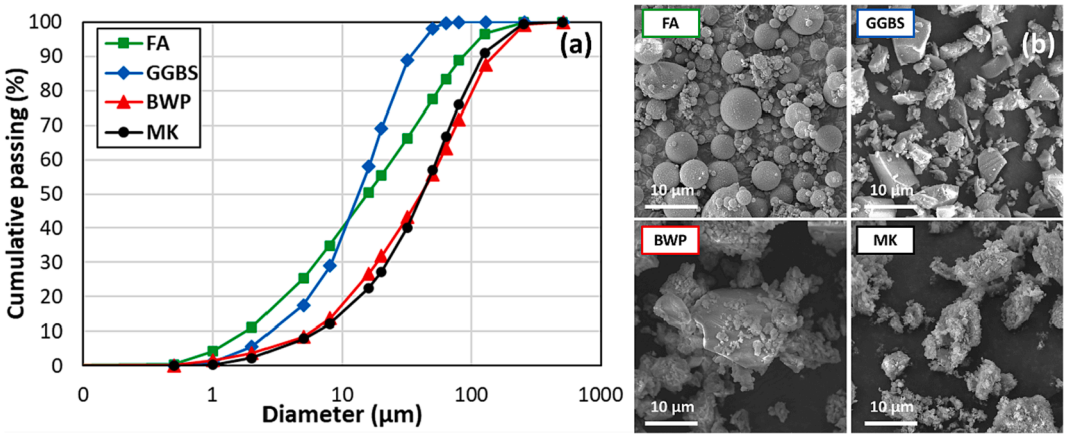

Fig. 1. Characterization of the powders selected as precursors: a) Particle size distribution; b) SEM observation using secondary electrons.

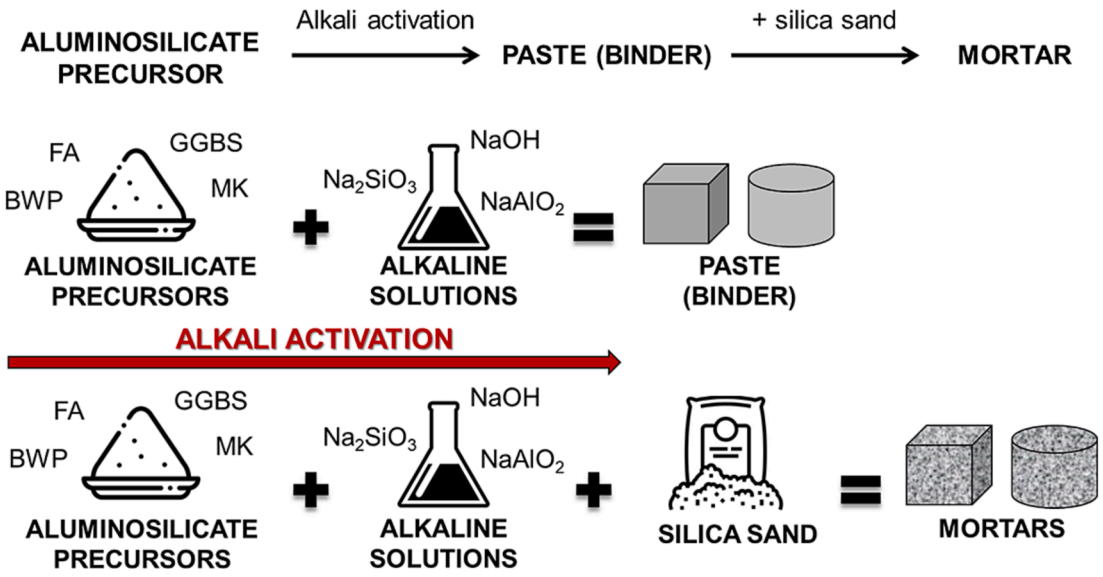

Fig. 2. Schematic representation of AAMs production chain.

Table 3
Mass compositions of the alkali-activated pastes and mortars and weight ratios between liquid and solid fractions.

Sample	Precursor	NaOH	8 M NaOH sol.	Sodium silicate sol.	Sodium aluminate	Extra water	Sand	Liquid/precursor
P-FA	68.9	–	5.2	25.9	–	–	–	0.26
P-GGBS	77.5	2.2	–	11.2	–	9.1	–	0.20
P-BWP	57.9	–	4.5	6.7	9.3	21.7	–	0.50
P-MK	52.3	4.4	–	43.3	–	–	–	0.41
M−FA	28.5	–	2.1	10.7	–	2.2	56.5	0.33
M−GGBS	29.5	0.9	–	4.3	–	6.4	58.9	0.30
M−BWP	26.8	–	2.1	3.1	4.3	10.1	53.6	0.50
M−MK	20.3	1.7	–	16.8	–	0.2	60.9	0.47

method proposed by Gilmore (2008) [41], under the hypotheses of secular equilibrium between ^{226}Ra-^{238}U and natural ^{235}U/^{238}U isotopic ratio. ^{238}U and ^{232}Th were then determined using the emissions of their radioactive daughters ^{226}Ra and ^{228}Ac/^{212}Pb.

According to the proprietary software used, the error associated to the concentration activities is defined as total uncertainty and it is computed at k = 1 confidence level (1σ). This parameter is obtained by propagating several uncertainty sources such as counting uncertainty, as the primary contribution, and efficiency related uncertainty among others.

The minimum detectable activity (CRMDA) was calculated according to the so-called Traditional ORTEC method available in GammaVision using equation (1):

$$CR_{MDA} = \frac{\frac{100}{SENS}\left(\sqrt{2 \bullet B_1 + \frac{2500}{SENS^2}} + \frac{50}{SENS}\right)}{LT} \quad (1)$$

where SENS is the Peak Cutoff value (%) on the Analysis tab (40 % in this work), B1 is the Peak background, and LT is the Live Time (sec).

Annex VIII of the Council Directive 2013/59/Euratom [23,25] defines the Activity Concentration Index (*I*) in order to quantify and regulate the exposure to gamma radiation originating from radionuclides in building materials (eq. (2):

$$I = \frac{C_{Ra226}}{300} + \frac{C_{Th232}}{200} + \frac{C_{K40}}{3000} \quad (2)$$

where C_{Ra226}, C_{Th232}, and C_{K40} are the activity concentrations of ^{226}Ra, ^{232}Th, and ^{40}K, respectively, expressed in Bq/kg as determined by gamma-ray spectrometry. An activity concentration index value of 1 is thus used as a conservative safety threshold below which building materials are radiologically safe, with 1 as the threshold dose corresponding to a maximum permissible value of 1 mSv per year) [42]. In practice, building materials are tested as safe when their I index is less than 1.

The explicit use of ^{226}Ra instead of its parent ^{238}U stands in the relative radiological impact they have. In natural radioactive families, though all the members are on average present, approaching or not secular equilibrium, the various radionuclides are not radiologically equivalent for type and energy of radiation emitted. As a result, in the case of ^{238}U family the most critical radionuclides are the ones from ^{226}Ra downward, due to its direct connection with ^{222}Rn, the main contributor to individual radiation dose and associated with remarkable radiation hazard from their alpha emissions. Radon, indeed, is a noble radioactive gas released from any rocks, soils, and derivatives at rates depending on the initial concentration of ^{226}Ra in the material and from its porosity under the influence of temperature, pressure, and moisture. Moreover, it further decays to a series of progeny radionuclides resulting in a complex multiple exposure covering both alpha and the most relevant gamma decays with the ^{238}U family [43].

Index *I*, therefore, provides a quick and practical approach to the easy selection of radiologically safe building materials, despite the multiple and complex radiological hazards they may represent.

2.3.2. *Multivariate analysis*

Comparison between AAMs, their precursors, and activators based on NORM data was carried out by PCA. PCA [44,45] is a consolidated chemometric technique that, based on a linear combination of the original variables (NORM activities in this case), rotates the spaces spanned by these variables in order to obtain a new space whose first versors (the principal component, PCs) carry most of the original

information (explained variance, EV%). In this way a 2D- or 3D-plot can fully describe the problem in terms of similarity or dissimilarity of samples and variables, and which variables mostly influence the samples' distribution.

In the present work, PCA was carried out with the software R (R Core Team, Vienna, Austria), using a homemade script.

3. Results and discussion

3.1. Radiometric data

Table 4 reports the radioactivity concentration (Bq/kg) of all the analyzed materials, ranging from the waste-based (FA, GGBS, and BWP) and natural (MK) precursors for alkali activation, up to intermediates, and final products. Reagents/components used in AAMs processing are also reported.

Reagents (NaOH, $NaAl_2O$, and Na_2SiO_3) include alkaline substances for the initial chemical attack of aluminosilicates and sand for their preparation as mortar. All the analyzed materials show very low NORM levels. It is expected in the case of NaOH, given its industrial production chain, while in the other cases, especially the ones containing silicates, it is not so straightforward, especially in the case of sand, as all these substances have a lithogenic origin and therefore contain variable NORM concentration levels. As for the sand triplicates we analyzed, the material employed revealed a very low NORM level. However, some further comments are reported below as they concern some general guidelines suitably commented to prevent potential and unexpected failures in radiological compliance.

The precursors reveal the highest value in activity concentrations of NORM, while activators and siliceous components are characterized by the minimum values of activity concentrations in natural radionuclides. Pastes and mortars, instead, reveal intermediate NORM levels resulting from the dilution brought by the used reagents. Overall, it is found that AAMs production in our experimental conditions brings an advantageous reduction in radiological hazard as compared to precursors, as shown in the resulting values of the dosimetric indices, in agreement with previous articles [4].

FA from coal energy production is long being used in building materials from cement and concrete up to bricks and tiles as well as AAMs [4] to reduce their disposal in landfills, given the overwhelming use of this fossil fuel to date [5]. Following the combustion process and the inherent solid mass reduction, coal ash is historically recognized as being enriched in inorganic and mineral components as compared to the parent fuel, including heavy metals and NORM, thus calling for careful management. For this reason, in this work, we found that, in agreement with past literature on the subject, including even the first EC document on the radioprotection concerning building materials [42], FA reveals not only the highest activity concentration values but, as expected, a dosimetric index of 1.74. Such value greatly exceeds the unit value threshold fixed by Euratom Directive, showing once more the long-recognized critical issues in FA as a building material. However, differently from FA use in cement and concrete, AAM processing efficiently solves the radiological issue, at least in our case, though some further comments and, what's relevant, some extra advice will be given later in this work.

GGBS is a milled blast furnace slag consisting of iron and steel by-products from iron production widely used in AAMs [4]. The sample herein analyzed shows a lower NORM content than FA, but higher than reported by Sofilić et al., [46], though the dosimetric index is well below the provided threshold. This means that, despite the huge databases available, owing to the remarkable variability in the natural composition of iron ores as well as of the industrial processes involved, the compliance with the radiological standards of Euratom Directive 2013/59 needs to be systematically checked in advance.

This statement is confirmed also by the radiometric data of BWP. In this case, the precursor material analyzed presents a NORM content comparable to GGBS, though with sensibly higher levels of ^{40}K leading to an I value larger than 1. This is not surprising, since, as described in the introduction, bricks and therefore their wastes will preserve the radiological fingerprints of the parent materials in all their geochemical diversity and independently from being natural or technogenic. It is worth noting that in our laboratory numerous samples of building materials (mostly tiles and their raw materials, but also AAMs are covered such as in Sas et al., 2019 [47]) are analyzed for NORM yearly for both research and commissioned purposes; in this framework on a set of 32 brick samples the mean value of I assessed ranged between 1.07 and 0.44 with an average of 0.73 ± 0.19 (unpublished data by Tositti et al.), while bricks produced from trachyte wastes a volcanic rock from the Euganean Hills investigated for potentially high rock radioactivity level or from ceramic sludge showed an I ranging between 0.53 and 0.82 [19].

MK typically serves as a natural reference for AAM production, though strictly speaking it is a derivative from kaolin minerals, basically pertaining to clays, from which metakaolin is obtained by thermal treatment [2,7].

Radioactivity in clays is highly variable as reported for example in Walley El-Dine et al., [48], who widely analyzed different samples from Egypt, but also from very distant locations, showing a strong dependency on clay source areas.

In our case, the activity concentrations of NORM measured are low, while e.g., Ivanovic et al., [49] found levels 4–5 times higher than ours.

Table 4
Results of radioactivity essays by high-resolution γ-ray spectrometry on all the materials. Dosimetric indices I, according to Euratom Directive 2013/59, calculated from radioactivity data, are also reported. All data represent averages of triplicate samples together with their standard deviation. All nuclides' concentrations and standard deviations are reported in Bq kg^{-1}.

	Materials	^{226}Ra	^{214}Bi	^{214}Pb	^{232}Th (^{228}Ac)	^{212}Pb	^{212}Bi	^{40}K	I
Precursors	**BWP**	172 ± 15	100 ± 5	116 ± 2	51 ± 7	48 ± 2	33 ± 17	914 ± 15	1.12 ± 0.07
	FA	274 ± 23	196 ± 7	237 ± 9	106 ± 12	113 ± 1	92 ± 16	831 ± 26	1.74 ± 0.08
	GGBS	137 ± 22	95 ± 11	108 ± 12	50 ± 6	49 ± 6	35 ± 10	230 ± 112	0.78 ± 0.14
	MK	69 ± 22	43 ± 16	48 ± 10	108 ± 15	113 ± 14	82 ± 8	203 ± 155	0.85 ± 0.19
Raw Materials	**Na_2SiO_3**	9 ± 2	4 ± 2	5 ± 1	7 ± 2	1 ± 0.2	13 ± 4	63 ± 13	0.07 ± 0.01
	$NaAlO_2$	15 ± 1	10 ± 2	9 ± 2	10 ± 5	2 ± 0.3	31 ± 16	38 ± 1	0.09 ± 0.02
	NaOH	29 ± 18	9 ± 8	7 ± 5	11 ± 9	3 ± 2	22 ± 13	170 ± 135	0.19 ± 0.13
Pastes	**P-BWP**	107 ± 9	67 ± 4	81 ± 7	40 ± 9	37 ± 1	55 ± 21	597 ± 20	0.75 ± 0.05
	P-FA	224 ± 16	134 ± 8	164 ± 11	81 ± 9	88 ± 5	67 ± 8	655 ± 34	1.39 ± 0.09
	P-GGBS	99 ± 4	69 ± 3	85 ± 1	35 ± 4	38 ± 2	29 ± 13	120 ± 7	0.55 ± 0.02
	P-MK	66 ± 16	31 ± 2	35 ± 4	74 ± 8	81 ± 8	77 ± 22	251 ± 33	0.69 ± 0.08
Mortars	**M−BWP**	42 ± 7	34 ± 2	42 ± 2	21 ± 6	22 ± 5	22 ± 14	334 ± 21	0.36 ± 0.03
	M−FA	10 ± 3	13 ± 1	16 ± 1	29 ± 4	28 ± 1	44 ± 6	135 ± 18	0.22 ± 0.01
	M−GGBS	54 ± 5	19 ± 1	25 ± 0.5	22 ± 4	20 ± 0.1	17 ± 3	152 ± 13	0.34 ± 0.03
	M−MK	15 ± 3	6 ± 0.4	9 ± 2	29 ± 2	29 ± 1	26 ± 10	144 ± 7	0.25 ± 0.01
	sand	17 ± 15	10 ± 5	9 ± 5	10 ± 3	8 ± 2	11 ± 3	220 ± 101	0.17 ± 0.08

Both series of values agree with the ranges measured by Walley El-Dine et al., [48], the latter however leading to $I > 1$ suggesting once more the need for accurate radioactivity checks before production, as for all the material of lithogenic origin, given the natural variability in composition, radionuclides included, within any type of mineral and derivatives.

It is interesting to note, from a radiological point of view that, despite an irradiation term that may remain high, if not adequately evaluated after experimental assessment, some researchers suggest how the production of a AAM, whatever it is its original natural radioactivity content, still presents an interesting advantage. Indeed, as revealed by Lu et al., [5], the processing of aluminosilicates into AAMs can be modified to improve the "sealing" effect on the material pores, thus blocking radon and its progeny emanation from the materials [50,51], especially in indoor environments, where radon buildup might represent significant radiological hazard upon inhalation in the case of limited ventilation [52]. Table 5 indicates that the results obtained in the present work in terms of radioactivity concentrations for the most commonly analyzed (^{226}Ra, ^{232}Th, and ^{40}K) radionuclides are in good agreement with those reported in previous literature. Geopolymers in Table 5 were ordered based on the chemical composition of the raw material reported in the cited reference, however, the origin of such raw materials is generally different from those used in the present work. This is an indication of the huge variability of the materials, generally wastes, that can be used to produce geopolymers.

As a final remark, we comment on the characterized raw materials. All the samples analyzed in this work have negligible NORM levels, showing the ability to act as "diluents" of the raw materials suggesting their favorable role in mitigating potential radiological hazards from the final products.

Again, we advise on the need of carefully checking sand, which may suffer from unexpected variability in NORM similarly to clay. As an example, we report what we have experimented in this work. Indeed, during the measurement of the samples of one of the AAMs, we noticed that one of the mortar replicates, despite extra measurements, produced excess outlier data. Upon check we found that in one single specimen we used a sand aliquot from a different batch, discovering that, despite being a standard material for its grain size, it was likely from a widely different geographical origin in respect to all the others herein investigated, confirming the need for extreme care in the materials used for mixtures.

Table 5
Comparison of radioactivity concentrations (in Bq kg^{-1}) for some of the analyzed radionuclides. Readers are referred to the cited work for Sample codes explanation.

Raw materials	Sample code	^{226}Ra	^{232}Th	^{40}K	Reference
	M−BWP	42 ± 7	21 ± 6	334 ± 21	This work
Red mud	**RM0**	69 ± 4	120 ± 5	88 ± 4	[53]
Clay sediments	**GP CRCCS**	12.3 ± 0.8	23 ± 1	320 ± 10	[54]
Clay sediments	**GC GRCCS**	12.0 ± 0.7	25 ± 1	283 ± 9	[54]
	M−FA	10 ± 3	29 ± 4	135 ± 18	This work
50 % cement + 50 % limestone	**N/15Wg-AAFA**	36.4 ± 0.97	68 ± 1	580 ± 20	[55]
50 % cement + 50 % fly ash	**Glass-AAS**	55 ± 1	23.7 ± 0.8	89 ± 5	[55]
Water potabilization sludge	**GP CRCWPS**	11.0 ± 0.5	17.9 ± 0.9	223 ± 8	[54]
Water potabilization sludge	**GP GRCWPS**	13.8 ± 0.6	17.2 ± 0.8	270 ± 98	[54]
	M−GGBS	54 ± 5	22 ± 4	152 ± 13	This work
Granulated blast furnace slag + 30 % red mud	**RM70**	200 ± 24	150 ± 13	292 ± 6	[53]
	M−MK	15 ± 3	29 ± 2	144 ± 7	This work
50 % cement + 50 % slag	**Wg-AAS**	49 ± 1	22.8 ± 0.7	77 ± 5	[55]
50 % cement + 50 % silica fume	**Glass-AAFA**	57 ± 3	62 ± 1	550 ± 10	[55]

3.2. Dosimetric index evolution throughout AAMs processing

More specific considerations can be drawn considering only the dosimetric index (*I*). Fig. 3 shows the boxplot of this variable for each material and associated intermediate (paste) and product (mortar); the statistics have been calculated on their replicates.

Fig. 3 shows that all mortar samples have a dosimetric index below the law limit of 1.0 (the red dashed line), such as the three activators and the sand samples. Precursors and pastes have, instead, different behaviors. BWP and FA precursors have *I* median values (1.11 and 1.69 respectively) above the recommended limit, GGBS is slightly below (0.72), and MK has a median value of 0.97, its mean *I* is not significantly different from the limit of 1.0 (at significance level 0.05). The pastes have *I* median values lower than 1.0, except for FA_P, whose *I* is 1.47. It is interesting to note that it is possible to follow the reaction chain of each sample (from left to right in Fig. 3): the precursor has the highest *I* median value, it decreases with the reaction to paste and then it reaches a minimum when the AAMs reaches the mortar form. The drop in this last passage can be also dramatic, as in the case of M_FA whose *I* median value reaches 0.22.

In general, it can be observed that, during the reaction chain to produce AAMs, the activity concentrations of all the analyzed nuclides significantly decrease. Such a drop is reflected in the corresponding drop of the activity index *I* and is particularly strong in the last passage from mortar to paste, when the mortars are mixed with silica sand. However, the decrease of some nuclides, ^{40}K and ^{226}Ra, is not always significant after the first reaction of the precursors with the alkali activators. This explains why the *I* median values of FA and MK show only a slight drop from precursors to pastes.

3.3. Multivariate analysis

The activity concentration data obtained for AAMs, precursors, and activators were used to compute a PCA model to evaluate the behavior of each analyzed nuclide along the reaction chain. The dataset is composed of 4 classes of AAMs and their corresponding precursors (BWP, FA, GGBS, and MK) and pastes, the activators (NaOH, Na_2SiO_3, and $NaAlO_2$), and two sand samples. Two samples of sand are included in this elaboration owing to the non-negligible influence this may have on the final AAMs in terms of NORM. As explained, compliance with the Euratom requisites for building materials is the result of the NORM mixtures from the various components. In the case of sand, our experience indicates the need to check for its NORM content since one presented a very low NORM level enabling efficient dilution of the NORM in the parent waste material, but the second one did not. Source area and therefore minor chemical components may play a very relevant role in terms of radioactivity safety.

Each sample was replicated 3 times, some of them were replicated 5 times due to uncertainties in the measurements. The final dataset was composed of 66 objects (replicates of the samples) and 8 variables (the 7 NORMs and the dosimetric index, *I*). Fig. 4 shows the biplot obtained for the PCA model. Biplot was obtained by scaling both scores and loadings to the interval (-1; +1), allowing both to show on the same plot.

The two principal components, PC1 and PC2, reported in Fig. 4, explain together 94.1 % of the total variance, therefore they represent almost the entire information contained in the data. All the variables, including *I*, are reported in the right portion of the graph, at positive values of PC1. There are also two well-discriminated groups of NORM variables, whose closeness in the graph indicates a strong correlation

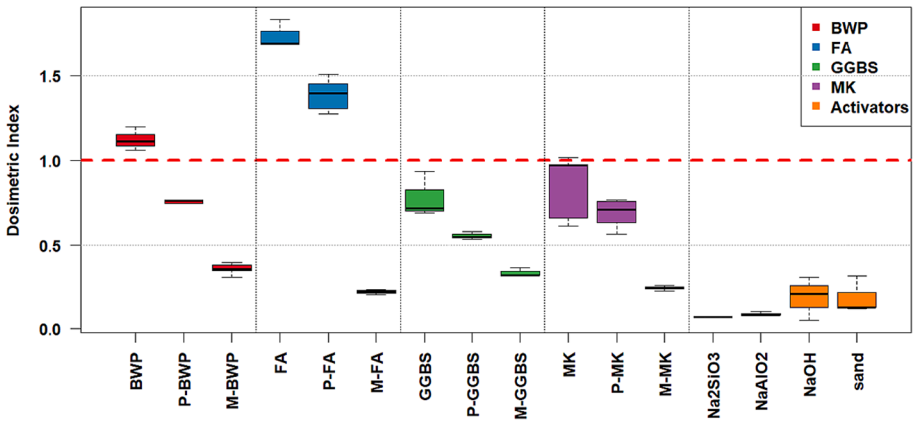

Fig. 3. Boxplots of the dosimetric index (I) for each sample. Colors indicate the precursor of each AAM family. The red horizontal line represents the dosimetric index limit of 1.0 according to Euratom Directive 2013/59.

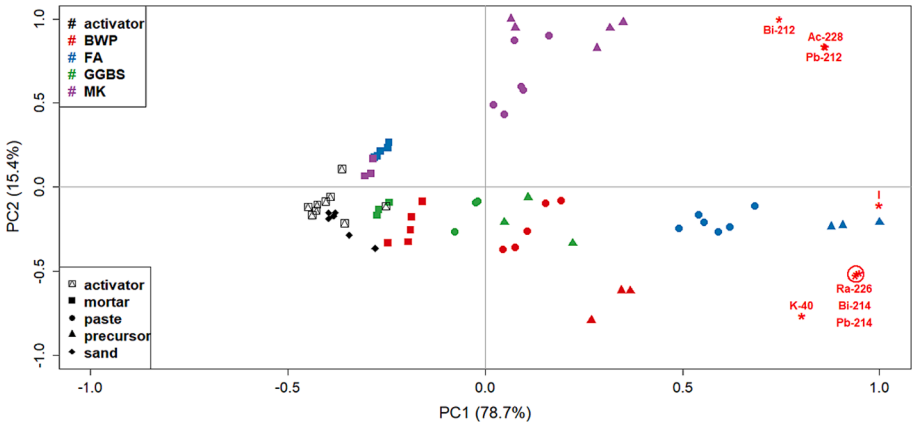

Fig. 4. Biplot of the pca model. red asterisks represent the variables, the other points represent the samples. objects are colored based on the aams family, while symbols represent the aams production stage: "precursor", "paste", and "mortar".

between them: the first group is composed of the main γ-emitters members of ^{232}Th family, i.e., ^{212}Bi, ^{212}Pb, and ^{228}Ac, the second one by those of ^{238}U, i.e.,^{226}Ra, ^{214}Bi, and ^{214}Pb, with a lower correlation also with ^{40}K.

The distribution of the variables in Fig. 4 indicates, in a qualitative way, that the samples placed in the left portion of the graph, at negative values of PC1, are the least concentrated in all radionuclides. In PCA, indeed, samples placed in the same quadrant of a certain variable are the most concentrated for that variable, while samples placed in the opposite quadrant of a certain variable are less concentrated. This is generally indicated as a "quadrant correspondence" between scores and loadings. Therefore, Fig. 4 shows that the activators have the lowest concentrations of all radionuclides. It can be observed that also the mortar samples (indicated by full squares) have lower concentrations for all radionuclides compared to the precursors (triangles) and the paste (circles) samples. Moreover, Fig. 4 makes it possible to follow the AAM production chain from right to left. As an example, the chain of BWP (in dark red) can be seen from the triangles in the lower part of the biplot, representing the precursor, to the paste samples (circles), and, finally, to the mortar products (squares). Such distribution pattern is generally true for all AAMs, except for some slight overlap between the precursors and the pastes (as for MK in purple). The biplot in Fig. 4 makes also possible to infer that the MK precursor and paste, due to their position at positive values of PC2, are mostly concentrated in ^{212}Bi, ^{212}Pb, and ^{228}Ac, while the other precursors are generally most concentrated in the other radionuclides. The variable *I* is placed in the middle of the two groups of radionuclides, since its computation requires the concentration of the two couples ^{212}Pb, ^{232}Th (^{228}Ac) and ^{226}Ra, ^{40}K. Its values are highest for FA precursor (light-blue squares) and all precursors in general.

4. Conclusions

A detailed study of the radioactivity redistribution patterns along the alkali-activated material (AAM) production chain has been carried out. Four distinct types of industrial solid wastes were used as precursor materials. Their granulometry was characterized in detail before starting the chemical processing to convert them into alkali-activated materials. Activity concentrations of all the materials were accurately characterized for NORM at all the stages by high-resolution gamma-ray spectrometry, and dosimetric indices based on EU Directive 2013/59 were calculated.

In all cases, based on the radiometric characterization of all the materials and reactants used, mortars, (i.e., the final AAM products), have been found to comply with the current European standards for radiological standards issued in the case of building materials. Radiometric indices, moreover, have been found to drop for all AAM families, ranging from higher (and, in some cases, not compliant with the law limits) values for precursors to lower values for the final AAMs suggesting that this strategy may be highly efficient for recycling purposes.

Multivariate analysis by PCA on the overall dataset, including all the radionuclides quantified by gamma-ray spectroscopy, allowed us to point out the efficient classification of alkali-activated materials before and after their chemical processing. Moreover, it was possible to evaluate the enrichment of specific radionuclides in each AAM family (in

particular from the decay chains of ^{232}Th and ^{238}U).

Finally, the present work provides recommendations and tips for optimal and safe exploitation of precursors in line with radioprotection standards.

Funding

This research did not receive any specific grant from funding agencies in the public, commercial, or not-for-profit sectors.

CRediT authorship contribution statement

Laura Tositti: Writing – review & editing, Writing – original draft, Validation, Supervision, Project administration, Funding acquisition, Conceptualization. **Giulia Masi:** Writing – review & editing, Writing – original draft, Validation, Methodology, Investigation. **Pietro Morozzi:** Writing – original draft, Validation, Methodology, Investigation, Formal analysis, Data curation. **Alessandro Zappi:** Writing – review & editing, Validation, Formal analysis, Data curation. **Maria Chiara Bignozzi:** Conceptualization, Funding acquisition, Project administration, Supervision, Validation, Writing – review & editing.

Declaration of Competing Interest

The authors declare that they have no known competing financial interests or personal relationships that could have appeared to influence the work reported in this paper.

Data availability

Data will be made available on request.

Acknowledgements

The authors would like to acknowledge Dr. Giovanni Ridolfi and Dr. Giuliana Bonvicini (Centro Ceramico, Sassuolo (MO), Italy) for laser granulometry and ICP-OES analyses, respectively.

References

[1] IPCC, IPCC AR6 Working Group 1: Summary for Policymakers | Climate Change The Physical Science Basis, (2021), accessed April 17, 2023, https://www.ipcc.ch/report/ar6/wg1/chapter/summary-for-policymakers/, 2021.
[2] H. Castillo, H. Collado, T. Droguett, M. Vesely, P. Garrido, S. Palma, State of the art of geopolymers: a review, E-Polymers 22 (2022) 108–124, https://doi.org/10.1515/EPOLY-2022-0015/ASSET/GRAPHIC/J_EPOLY-2022-0015_FIG_009.JPG.
[3] M. Valente, M. Sambucci, A. Sibai, Geopolymers vs. cement matrix materials: how nanofiller can help a sustainability approach for smart construction applications—a review, Nanomater. 2021, Vol. 11, Page 2007. 11 (2021) 2007. doi:10.3390/NANO11082007.
[4] M. Elzeadani, D.V. Bompa, A.Y. Elghazouli, One part alkali activated materials: a state-of-the-art review, J. Build. Eng. 57 (2022), 104871, https://doi.org/10.1016/J.JOBE.2022.104871.
[5] X. Lu, B. Liu, Q. Zhang, Q. Wen, S. Wang, K. Xiao, S. Zhang, E. Mokrzycki, A. Uliasz-Boché, X. Lu, B. Liu, Q. Zhang, Q. Wen, S. Wang, K. Xiao, S. Zhang, Recycling of coal fly ash in building materials: a review, Miner. 2023, Vol. 13, Page 25. 13 (2022) 25. doi:10.3390/MIN13010025.
[6] G. Masi, S. Manzi, M.C. Bignozzi, Gender balance in construction material research: the analysis of alkali-activated materials by a bibliometric study using scopus database, Front. Mater. 7 (2020) 321, https://doi.org/10.3389/FMATS.2020.572514/BIBTEX.
[7] Y. Wu, B. Lu, T. Bai, H. Wang, F. Du, Y. Zhang, L. Cai, C. Jiang, W. Wang, Geopolymer, green alkali activated cementitious material: synthesis, applications and challenges, Constr. Build. Mater. 224 (2019) 930–949, https://doi.org/10.1016/J.CONBUILDMAT.2019.07.112.
[8] J.L. Provis, Alkali-activated materials, Cem. Concr. Res. 114 (2018) 40–48, https://doi.org/10.1016/J.CEMCONRES.2017.02.009.
[9] S.A. Bernal, E.D. Rodríguez, A.P. Kirchheim, J.L. Provis, Management and valorisation of wastes through use in producing alkali-activated cement materials, J. Chem. Technol. Biotechnol. 91 (2016) 2365–2388, https://doi.org/10.1002/JCTB.4927.
[10] C. Shi, B. Qu, J.L. Provis, Recent progress in low-carbon binders, Cem. Concr. Res. 122 (2019) 227–250, https://doi.org/10.1016/J.CEMCONRES.2019.05.009.
[11] B.C. McLellan, R.P. Williams, J. Lay, A. Van Riessen, G.D. Corder, Costs and carbon emissions for geopolymer pastes in comparison to ordinary portland cement, J. Clean. Prod. 19 (2011) 1080–1090, https://doi.org/10.1016/J.JCLEPRO.2011.02.010.
[12] P. Cong, Y. Cheng, Advances in geopolymer materials: a comprehensive review, J. Traffic Transp. Eng. (english Ed.) 8 (2021) 283–314, https://doi.org/10.1016/J.JTTE.2021.03.004.
[13] B. Kim, J. Lee, J. Kang, W. Um, Development of geopolymer waste form for immobilization of radioactive borate waste, J. Hazard. Mater. 419 (2021), 126402, https://doi.org/10.1016/J.JHAZMAT.2021.126402.
[14] D.C. Wilson, L. Rodic, A. Scheinberg, C.A. Velis, G. Alabaster, Comparative analysis of solid waste management in 20 cities, Waste Manag. Res. 30 (2012) 237–254, https://doi.org/10.1177/0734242X12437569/ASSET/IMAGES/LARGE/10.1177_0734242X12437569-FIG6.JPEG.
[15] B. Michalik, A. Dvorzhak, R. Pereira, J. Lourenço, H. Haanes, C. Di Carlo, C. Nuccetelli, G. Venoso, F. Leonardi, R. Trevisi, F. Trotti, R. Ugolini, L. Pannecoucke, P. Blanchart, D. Perez-Sanchez, A. Real, A. Escribano, L. Fevrier, A. Kallio, L. Skipperud, S.M. Jerome, J.M. Popic, A methodology for the systematic identification of naturally occurring radioactive materials (NORM), Sci. Total Environ. 881 (2023), 163324, https://doi.org/10.1016/J.SCITOTENV.2023.163324.
[16] J.H. Schön, Rocks-their classification and general properties, Dev. Pet. Sci. 65 (2015) 1–19, https://doi.org/10.1016/B978-0-08-100404-3.00001-9.
[17] R.H. Wilkens, Physical properties of rocks: fundamentals and principles of petrophysics, Eos Trans. Am. Geophys. Union 78 (1997) 600, https://doi.org/10.1029/97EO00363.
[18] R. Trevisi, F. Leonardi, S. Risica, C. Nuccetelli, Updated database on natural radioactivity in building materials in Europe, J. Environ. Radioact. 187 (2018) 90–105, https://doi.org/10.1016/J.JENVRAD.2018.01.024.
[19] C. Coletti, E. Brattich, G. Cinelli, G. Cultrone, L. Maritan, C. Mazzoli, D. Mostacci, L. Tositti, R. Sassi, Radionuclide concentration and radon exhalation in new mix design of bricks produced reusing NORM by-products: the influence of mineralogy and texture, Constr. Build. Mater. 260 (2020), 119820, https://doi.org/10.1016/J.CONBUILDMAT.2020.119820.
[20] G. Cinelli, B. Capaccioni, M.A. Hernández-Ceballos, D. Mostacci, A. Perghem, L. Tositti, Radiological risk from thoron, a case study: the particularly radon-prone area of Bolsena, and the lesson learned, Radiat. Phys. Chem. 116 (2015) 381–385, https://doi.org/10.1016/J.RADPHYSCHEM.2015.02.016.
[21] B. Capaccioni, G. Cinelli, D. Mostacci, L. Tositti, Long-term risk in a recently active volcanic system: evaluation of doses and indoor radiological risk in the quaternary Vulsini Volcanic District (Central Italy), J. Volcanol. Geoth. Res. 247–248 (2012) 26–36, https://doi.org/10.1016/J.JVOLGEORES.2012.07.014.
[22] COST Action TU1301 NORM4BUILDING, Naturally occurring radioactive materials in construction: Integrating radiation protection in reuse, (2017) 338.
[23] Unscear, Sources and Effects of Ionizing Radiation Volume I: source, United Nations Sci, Committe Eff. at. Radiat. I (2000) 1–654. //www.unscear.org/unscear/en/publications/2000_1.html (accessed April 3, 2023.
[24] L.C. Damonte, P.C. Rivas, A.F. Pasquevich, F. Andreola, F. Bondioli, A.M. Ferrari, L. Tositti, G. Cinelli, Structural characterization of natural and processed zircons with X-rays and nuclear techniques, Adv. Condens. Matter Phys. 2017 (2017), https://doi.org/10.1155/2017/9707604.
[25] European Council, Council Directive 2013/59/Euratom of 5 December 2013 laying down basic safety standards for protection against the dangers arising from exposure to ionising radiation, and repealing Directives 89/618/Euratom, 90/641/Euratom, 96/29/Euratom, 97/43/Euratom a, Queen's Printer of Acts of Parliament, 2013. https://webarchive.nationalarchives.gov.uk/eu-exit/https://eur-lex.europa.eu/legal-content/EN/TXT/?uri=CELEX:02013L0059-20140117 (accessed April 17, 2023).
[26] M. Łach, M. Hebdowska-Krupa, A. Stefańska, J. Stefanek, A. Stanek, J. Mikuła, M. Hebda, Characterisation of post-production raw material from the Raciszyn II deposit as a material suitable for the production of alkaline-activated materials, J. Therm. Anal. Calorim. 138 (2019) 4551–4559, https://doi.org/10.1007/s10973-019-08539-4.
[27] T. Hertel, Y. Pontikes, Geopolymers, inorganic polymers, alkali-activated materials and hybrid binders from bauxite residue (red mud) – putting things in perspective, J. Clean. Prod. 258 (2020), 120610, https://doi.org/10.1016/j.jclepro.2020.120610.
[28] M.M. Alonso, C. Gascó, M.M. Morales, J.A. Suárez-Navarro, M. Zamorano, F. Puertas, Olive biomass ash as an alternative activator in geopolymer formation: a study of strength, radiology and leaching behaviour, Cem. Concr. Compos. 104 (2019), 103384, https://doi.org/10.1016/j.cemconcomp.2019.103384.
[29] J. Temuujin, A. Minjigmaa, B. Davaabal, U. Bayarzul, A. Ankhtuya, T. Jadambaa, K.J.D. MacKenzie, Utilization of radioactive high-calcium Mongolian flyash for the preparation of alkali-activated geopolymers for safe use as construction materials, Ceram. Int. 40 (2014) 16475–16483, https://doi.org/10.1016/j.ceramint.2014.07.157.
[30] Z. Sas, W. Sha, M. Soutsos, R. Doherty, D. Bondar, K. Gijbels, W. Schroeyers, Radiological characterisation of alkali-activated construction materials containing red mud, fly ash and ground granulated blast-furnace slag, Sci. Total Environ. 659 (2019) 1496–1504, https://doi.org/10.1016/j.scitotenv.2019.01.006.
[31] T. Croymans, W. Schroeyers, P. Krivenko, O. Kovalchuk, A. Pasko, M. Hult, G. Marissens, G. Lutter, S. Schreurs, Radiological characterization and evaluation of high volume bauxite residue alkali activated concretes, J. Environ. Radioact. 168 (2017) 21–29, https://doi.org/10.1016/j.jenvrad.2016.08.013.

[32] Parlamento Italiano, DECRETO LEGISLATIVO 31 luglio 2020, n. 101, 2020. https://www.gazzettaufficiale.it/eli/id/2020/08/12/20G00121/sg (accessed April 17, 2023).
[33] E. Sassoni, P. Pahlavan, E. Franzoni, M.C. Bignozzi, Valorization of brick waste by alkali-activation: a study on the possible use for masonry repointing, Ceram. Int. 42 (2016) 14685–14694, https://doi.org/10.1016/J.CERAMINT.2016.06.093.
[34] J.L. Provis, K. Arbi, S.A. Bernal, D. Bondar, A. Buchwald, A. Castel, S. Chithiraputhiran, M. Cyr, A. Dehghan, K. Dombrowski-Daube, A. Dubey, V. Ducman, G.J.G. Gluth, S. Nanukuttan, K. Peterson, F. Puertas, A. van Riessen, M. Torres-Carrasco, G. Ye, Y. Zuo, RILEM TC 247-DTA round robin test: mix design and reproducibility of compressive strength of alkali-activated concretes, Mater. Struct. Constr. 52 (2019) 1–13, https://doi.org/10.1617/S11527-019-1396-Z/FIGURES/6.
[35] R. San Nicolas, M. Cyr, G. Escadeillas, Characteristics and applications of flash metakaolins, Appl. Clay Sci. 83–84 (2013) 253–262, https://doi.org/10.1016/J.CLAY.2013.08.036.
[36] R. Pouhet, M. Cyr, R. Bucher, Influence of the initial water content in flash calcined metakaolin-based geopolymer, Constr. Build. Mater. 201 (2019) 421–429, https://doi.org/10.1016/J.CONBUILDMAT.2018.12.201.
[37] G. Masi, Steel corrosion behavior in light weight fly-ash based alkali activated mortars, Appl. Sci. 2021, Vol. 11, Page 1908. 11 (2021) 1908. doi:10.3390/APP11041908.
[38] L. Carabba, S. Pirskawetz, S. Krüger, G.J.G. Gluth, M.C. Bignozzi, Acoustic emission study of heat-induced cracking in fly ash-based alkali-activated pastes and lightweight mortars, Cem. Concr. Compos. 102 (2019) 145–156, https://doi.org/10.1016/J.CEMCONCOMP.2019.04.013.
[39] W.D.A. Rickard, R. Williams, J. Temuujin, A. van Riessen, Assessing the suitability of three Australian fly ashes as an aluminosilicate source for geopolymers in high temperature applications, Mater. Sci. Eng. A 528 (2011) 3390–3397, https://doi.org/10.1016/J.MSEA.2011.01.005.
[40] The British Standard Institution, BS EN 196-1:2016 Methods of testing cement. Determination of strength, (2016). https://www.thenbs.com/PublicationIndex/documents/details?Pub=BSI&DocID=314246 (accessed April 3, 2023).
[41] G.R. Gilmore, Practical Gamma-Ray Spectrometry: Second Edition, Pract. Gamma-Ray Spectrom. Second Ed. (2008) 1–387. doi:10.1002/9780470861981.
[42] D.-G. for E. European Commission, Radiological protection principles concerning the natural radioactivity of building materials, (2000). https://op.europa.eu/en/publication-detail/-/publication/988f3243-5259-43a5-b621-fbff662deeb0/language-en (accessed April 3, 2023).
[43] W. Burkart, Radon and its decay products in the indoor environment: radiation exposure and risk estimation., in: Adv. Aerobiol. Exp. Suppl., Birkhäuser, Basel, 1987: pp. 303–310. doi:10.1007/978-3-0348-7491-5_51/COVER.
[44] R. Bro, A.K. Smilde, Principal component analysis, Anal. Methods 6 (2014) 2812–2831, https://doi.org/10.1039/c3ay41907j.
[45] A. Zappi, V. Marassi, S. Giordani, N. Kassouf, B. Roda, A. Zattoni, P. Reschiglian, D. Melucci, Extracting information and enhancing the quality of separation data: a review on chemometrics-assisted analysis of volatile, soluble and colloidal samples, Chemosensors. 11 (2023), https://doi.org/10.3390/CHEMOSENSORS11010045.
[46] T. Sofilić, D. Barišić, U. Sofilić, Natural radioactivity in steel slag aggregate, Arch. Metall. Mater. 56 (2011) 627–634.
[47] Z. Sas, N. Vandevenne, R. Doherty, R. Vinai, J. Kwasny, M. Russell, W. Sha, M. Soutsos, W. Schroeyers, Radiological evaluation of industrial residues for construction purposes correlated with their chemical properties, Sci. Total Environ. 658 (2019) 141–151, https://doi.org/10.1016/J.SCITOTENV.2018.12.043.
[48] N.W. El-Dine, A. Sroor, A. El-Shershaby, S.M. El-Bahi, F. Ahmed, Radioactivity in local and imported kaolin types used in Egypt, Appl. Radiat. Isot. 60 (2004) 105–109, https://doi.org/10.1016/J.APRADISO.2003.09.006.
[49] M. Ivanovic, L. Kljajevic, M. Nenadovic, N. Bundaleski, I. Vukanac, B. Todorovic, S. Nenadovic, Physicochemical and radiological characterization of kaolin and its polymerization products, Mater. Construcción. 68 (2018) e155–e, https://doi.org/10.3989/MC.2018.00517.
[50] K. Gijbels, P. Krivenko, O. Kovalchuk, A. Pasko, S. Schreurs, Y. Pontikes, W. Schroeyers, The influence of porosity on radon emanation in alkali-activated mortars containing high volume bauxite residue, Constr. Build. Mater. 230 (2020), 116982, https://doi.org/10.1016/J.CONBUILDMAT.2019.116982.
[51] D. Hatungimana, C. Taşköprü, M. İçhedef, M.M. Saç, Ş. Yazıcı, Compressive strength, water absorption, water sorptivity and surface radon exhalation rate of silica fume and fly ash based mortar, J. Build. Eng. 23 (2019) 369–376, https://doi.org/10.1016/J.JOBE.2019.01.011.
[52] W.W. Nazaroff, A.V. Nero, Radon and its decay products in indoor air, J, Wiley, 1988.
[53] Z. Luo, Y. Hao, Y. Mu, C. Tang, X. Liu, Solidification/stabilization of red mud with natural radionuclides in granular blast furnace slag based geopolymers, Constr. Build. Mater. 316 (2022), 125916, https://doi.org/10.1016/j.conbuildmat.2021.125916.
[54] S.S. Nenadović, C. Ferone, M.T. Nenadović, R. Cioffi, M.M. Mirković, I. Vukanac, L. M. Kljajević, Chemical, physical and radiological evaluation of raw materials and geopolymers for building applications, J. Radioanal. Nucl. Chem. 325 (2020) 435–445, https://doi.org/10.1007/s10967-020-07250-1.
[55] F. Puertas, M.M. Alonso, M. Torres-Carrasco, P. Rivilla, C. Gasco, L. Yagüe, J. A. Suárez, N. Navarro, Radiological characterization of anhydrous/hydrated cements and geopolymers, Constr. Build. Mater. 101 (2015) 1105–1112, https://doi.org/10.1016/j.conbuildmat.2015.10.074.